S. Afshan, M. Theofanous, J. Wang, M. Gkantou, L. Gardner. (2019) Testing, numerical simulation and design of prestressed high strength steel arched trusses. Engineering Structures; **183** 510–522.

Testing, numerical simulation and design of prestressed high strength steel arched trusses

S. Afshan [(1)*], M. Theofanous [(2)], J. Wang [(3)], M. Gkantou [(4)], L. Gardner [(5)]

(1) Brunel University London, UK
(2) Birmingham University, UK
(3) University of Bath, UK
(4) Liverpool John Moores University, UK
(5) Imperial College London, UK

Abstract

The structural behaviour of prestressed high strength steel arched trusses is studied in this paper through experimentation and numerical modelling. Four 11 m span prestressed arched trusses fabricated from S460 hot finished square hollow section members were loaded vertically to failure. Three of the tested trusses were prestressed to different levels by means of a 7-wire strand cable housed within the bottom chord, while the fourth truss contained no cable and served as a control specimen. Each truss was loaded at five points coinciding with joint locations along its span, and the recorded load-deformation responses at each loading point are presented. Inclusion and prestressing of the cable was shown to delay yielding of the bottom chord and enhance the load carrying capacity of the trusses, which ultimately failed by either in-plane or out-of-plane buckling of the top chord. For the tested trusses, around 40% increases in structural resistance were achieved through the addition of the cable, though the self-weight was increased by only approximately 3%. In parallel with the experimental programme, a finite element model was developed and validated against the test results. Upon successful replication of the experimentally observed structural response of the trusses, parametric studies were conducted to investigate the effect of key parameters such as prestress level, material grade and the top chord cross-section on the overall structural response. Based on both the experimental and numerical results, design recommendations in the form of simple design checks to be performed for such systems are provided.

Key words

Cable-in-tube system; Experimentation; Finite element modelling; High strength steel; Prestressing; Testing; Trusses.

1. Introduction

Steels with yield strengths higher than 460 MPa are considered to be high strength within European construction practice; the design of high strength steel structures up to S700 is currently covered by EN 1993-1-12 [1]. The main benefit of using high strength steel (HSS) as a structural material is that it enables smaller cross-sections to be employed which, in turn, leads to reduced depletion of resources, reduced structural self-weight and hence smaller

foundation sizes, with direct savings in construction, transportation and erection costs. Several studies into the behaviour and design of high strength steel cross-sections and members in compression and bending have been carried out [2-10] to underpin the development of design rules and facilitate wider use in structural applications. However, these studies have generally only considered the response of individual elements; in the present investigation, the use of high strength steel in arched trusses, in conjunction with prestressing cables to enhance load-carrying capacity and reduce self-weight and deflections is explored. Reduction in self-weight is particularly important in long-span structures where the weight of the structure becomes an increasing proportion of the total load to be borne; the studied systems would therefore be well suited to such applications.

Work on prestressed steel structures dates back to 1950 when Magnel [11] explored the savings that could arise from prestressing steel structures. Belenya [12] analysed the behaviour of prestressed load-bearing structures, while Ellen [13] patented a technique of erecting arched trusses with sliding joints through prestressing of a cable, which then forms part of the load-bearing structure. Stressed-arch frames which have emerged as a promising structural system appropriate for long unsupported spans were extensively studied in Australia several decades ago [14-17]. The behaviour of prestressed beams [18-21], columns [22-23], trusses [24-28] and frames [29-30] has also been explored. A number of recent studies of steel structures in which cables are housed within hollow sections have been carried out [31-33]; this provides a practical means of prestressing, while also protecting the cables. These structural systems, the overall response of which is the subject of the present paper, have found several applications in practice, including the Central West Livestock Exchange in Forbes and the Sydney Olympic Stadium reconfiguration in Homebush, both developed by the company S-Squared [34]. Components of the trusses examined herein have also been tested individually in tension and compression, as reported in [35].

In the present paper, an experimental study into the behaviour of prestressed trusses with a focus on their response under gravity loading is reported in Section 2, where the testing arrangement, specimen details, instrumentation and results are described. A numerical modelling investigation, performed in parallel with the experimental programme, is presented in Section 3, while utilising both the experimental and the numerical modelling results, design recommendations for prestressed high strength steel trusses are presented in Section 4.

2. Laboratory testing

2.1 Geometric and material properties of test specimens

A total of four high strength steel arched trusses spanning over a length of 11 m were tested to failure. One truss had no prestressing cable and was used as a control specimen, while the remaining three trusses had a 7-wire strand prestressing cable with a nominal yield strength of 1860 N/mm^2, designated as Y1860S7 according to [36], embedded within their bottom chord. The cables were prestressed to varying load levels, to allow an assessment of the effect of prestress on the response of the trusses to be carried out. The trusses were fabricated from hot finished square hollow sections (SHS) in Grade S460 steel [37]. The top and bottom chord

elements were SHS 70×70×6.3 and SHS 50×50×5 respectively, while the vertical and diagonal elements were SHS 40×40×2.9, apart from those at the end supports which were SHS 50×50×5. All the adopted high strength steel tubular elements were Class 1 according to the EN 1993-1-1 [38] classification limits, to avoid premature failure by local buckling. All joints between the various truss elements were made using full penetration butt welds. The overall configuration of the assembled arched trusses is shown in Fig. 1. For ease of transportation, each truss was fabricated in three pieces, which were assembled in the Structures Laboratory at Imperial College London by bolting together the construction joints (Labelled EP1 and EP2 in Fig. 1).

Accurate measurements of the geometric dimensions of the individual tubular truss elements were carried out prior to testing. The average measured dimensions for each of the section sizes are reported in Table 1, and since no significant variation in the measured dimensions were observed between trusses, the same values were assumed for all 4 trusses. In Table 1, h is the section depth, b is the section width, t is the section thickness and r_i is the internal corner radius. The material properties of the steel sections and the prestressing cables were obtained by means of tensile tests; a full description of the material tests is provided in [8, 35] while a summary of the key results is reported in Table 2, where E is the Young's modulus, f_y is the yield strength, f_u is the ultimate tensile strength, ε_u is the strain at the ultimate tensile strength and ε_f is the plastic strain at fracture (based on an original standard gauge length of $L_0 = 5.65\sqrt{A_c}$, where A_c is the cross-sectional area of the coupon).

The steel truss with no prestressing cable, denoted as Truss 1, was used as a control specimen. The remaining three trusses had cables embedded in their bottom chords, which were prestressed to 5 kN (nominal prestress to remove slack), 0.5 P_{opt} and P_{opt} for Trusses 2, 3 and 4 respectively. The optimal prestress P_{opt} is defined by Eq. (1), and corresponds to the prestress force that causes the cable and the steel tube to yield simultaneously when subjected to tension [33]. In Eq. (1), A, E and f_y are the cross-sectional area, Young's modulus and yield strength, respectively, while the subscripts c and t refer to the cable and the steel tube.

$$P_{opt} = \left(\frac{A_c A_t}{A_t E_t + A_c E_c}\right)\left(f_{cy} E_t - f_{ty} E_c\right) \quad \text{but } P_{opt} \le A_t f_{ty} \text{ and } A_c f_{yc} \tag{1}$$

The measured geometric and material properties of the bottom chord tube (SHS 50×50×5) and the prestressing cable were: A_c = 151 mm^2, A_t = 858 mm^2, E_c = 130000 N/mm^2, E_t = 210000 N/mm^2, f_{cy} = 1703 N/mm^2 and f_{ty} = 505 N/mm^2; these properties were used to determine the optimal prestress force from Eq. (1) of P_{opt} = 189 kN.

2.2 Test set-up and instrumentation

The tests were carried out in the purpose-built rig depicted in Fig. 2. Vertical downward loading was applied via hydraulic jacks to each truss at five points along on the bottom chord at the locations shown in Fig. 2(a). Steel plates welded to the bottom chords of the trusses at the specified loading locations were utilised to connect the loading jacks, each with a maximum capacity of 300 kN, to the trusses, as shown in Fig. 3. The trusses were supported on two

concrete blocks, which were in turn secured to the strong floor of the laboratory. Simply supported conditions were achieved by means of steel rollers located at the ends of the trusses that allowed axial displacement of the truss ends, as depicted in Fig. 4. A series of lateral restraints was provided to the top chords of the trusses at the joint locations, as shown in Fig. 2, ensuring a global in-plane response. The details of the connections of the cable to the truss and the test rig are shown in Fig. 5.

All truss specimens were extensively instrumented as schematically shown in Fig. 2(a). A total of five string potentiometers attached to the bottom chord of the trusses at a distance of 100 mm from each of the five loading points were utilised to measure the vertical downward deflection of the truss specimens during the tests. Electrical resistance strain gauges, placed in pairs on the top and bottom truss chord elements, were used to measure the longitudinal strain during both the prestressing and loading stages. Three pairs of strain gauges were placed on the top chord, while four pairs of strain gauges were used for the bottom chord, the locations of which are shown in Fig. 2(a). The rotations of the trusses at the two ends were measured using inclinometers, while two linear variable differential transducers (LVDT) were adopted to measure the axial displacement during loading. The force in the prestressing cables was monitored during the tests with using two load cells located at the two end anchorage points, as shown in Fig. 2.

2.3 Prestressing and load application

The truss specimens were prestressed in the Structures Laboratory at Imperial College London prior to testing. The prestressing cables, located within the bottom chord of the fully assembled trusses, were first anchored in place at both ends and then stressed using a PT30-6PS jack, as shown in Fig. 6. Load cells were placed at the two ends of the trusses to monitor the applied force during prestressing. Once the required prestress level was reached, the loading jack was removed and the wedges at the stressing end were hammered in to reduce the prestress loss due to anchorage slip upon jack removal. The measured and the target prestress values for each of the tested trusses are reported in Table 3. The difference between the measured and target prestress is associated with the loss of prestress upon jack removal. For safety reasons, the maximum prestress load applied, before removal of the jack, was limited to about 80% of the cable yield load (255 kN). Note that the cables were not grouted in place in the present study, though grouting is often used in practice as a means of bonding the cable to the surrounding structure and of protecting the cable against corrosion [33].

Following prestressing, the trusses were loaded vertically by five equal point loads, F_1, F_2, F_3, F_4 and F_5, at a rate of 5 kN/min per point load. The tests were paused at suitable intervals to adjust the length of the lateral support cables to ensure that they remained taut and the truss deformations remained in-plane. Applied load, end rotation, strain, vertical displacement, cable force and axial displacement at the supports were all recorded at 1 second intervals using the data acquisition system DATASCAN and logged using the DSLOG computer package.

2.4 Results and discussion

The measured load versus vertical displacement responses recorded at each of the loading points, are shown in Figs. 7(a) – 7(d) for Trusses 1 to 4 respectively. Owing to the symmetric loading arrangement, the recorded load-displacement responses at loading points 1 and 2 is similar to that recorded at loading points 5 and 4 respectively. In order to assess the effect of the cable and the applied prestress level on the overall structural response, the applied vertical load versus the recorded mid-span (loading point 3) deflection of all the tested specimens are shown in Fig. 8. As expected, Truss 1, which had no prestressing cable, failed by yielding of the bottom chord. In the Truss 2 and Truss 4 tests, in-plane failure modes were observed, as shown in Fig. 9(a), where the failure occurred due to buckling of one of the top chord members within the plane of the truss. Truss 3 showed evidence of out-of-plane deformations (Fig. 9(b)) of the top chord, limiting the ultimate failure load, as can be seen from Fig. 8. The yield load, defined as the load corresponding to the end of the elastic range, and the maximum load achieved, in each of the tested trusses are summarised in Table 4. Note that the values reported in Table 4 are the sums of the loads at the five loading points. It may be seen from Table 4 that the application of higher levels of prestress extends the elastic range, providing improved serviceability performance, but brings the yield and ultimate loads of the system closer together, which may mean less warning of impending failure. On the other hand, a ductile response can still be attained by ensuring that yielding of the lower chord in tension rather than buckling of the upper chord in compression is the governing failure condition, as discussed further in Section 4.

Analytical predictions of the mid-span load-displacement responses, employing the measured geometric and material properties of the trusses, were also derived, and are depicted in Fig. 8. Firstly, a relationship between the mid-span vertical load and the bottom chord tensile axial force was established by considering the static equilibrium state of the truss. The bottom chord tensile axial force was then set to two limiting load values corresponding to (1) the point at which the bottom chord tube yields while the cable is still in the linear elastic range, $N_{y,bot}$, as given as a function of initial prestress level by Eq. (2) and (2) the point at which both the bottom chord tube and cable yield, $N_{u,bot}$ as given by Eq. (3). The total vertical loads (i.e. the sum of F_1 to F_5) corresponding to these two limiting axial forces in the bottom chords were then taken as the yield load and the ultimate load of the truss assembly. These limiting points are shown in Fig. 8 for Truss 3. The analytical total load-mid-span displacement response for each of the trusses was set to follow the pre-yield stiffness of the truss prior to the yield load limit and the post-yield stiffness of the truss up to the ultimate load limit. The pre-yield and post-yield stiffnesses were obtained from numerical models of the tested trusses which were simulated in ABAQUS [39], as described in Section 3.

$$N_{y,bot} = \left(P_i + A_t f_{ty}\right)\left(1 + \frac{E_c A_c}{E_t A_t}\right) \tag{2}$$

$$N_{u,bot} = A_t f_{ty} + A_c f_{cy} \tag{3}$$

The influence of the addition of the prestressing cable and the application of prestress may be seen from the load-deformation responses in Fig. 8 and the ultimate loads reported in Table 4. With the addition of the cable, the ultimate loads of Trusses 2, 3 and 4 were limited by buckling of the top-chord and displayed a significant increase of around 40% over Truss 1, where failure was governed by yielding of the bottom chord. Increasing the prestress level from 5.9 kN (in Truss 2) to 149.9 kN (in Truss 4) is shown to effectively extend the elastic range of the truss by delaying yielding of the steel tube in the bottom chord, resulting in a reduction in mid-span displacement at failure of approximately 50%. The substantial improvements in structural performance were accompanied by an increase in self-weight of just 3%, due to the introduction of the cable. It should be noted that for different truss geometries and material grades, the level of improvement in the load carrying capacity and deformation at failure will of course vary. This is investigated by means of extensive numerical parametric studies in the following section.

3. Numerical modelling

A numerical modelling study was performed in parallel with the experimental investigation to examine further the structural response of prestressed high strength steel arched trusses. The experimental results presented in Section 2 are used to validate the numerical models, which are subsequently used to perform parametric studies. The development of the numerical models along with the results of the parametric studies are described hereafter.

3.1 Development of FE models

The general-purpose finite element analysis package ABAQUS [39] was employed throughout the numerical study. Two numerical models of the trusses were developed in order to investigate the influence of element type on the structural response. The models were: (i) a model with beam elements for the truss members and truss elements for the cable (denoted Model B) and (ii) a model with shell elements for the truss members and solid elements for the cable (denoted Model S). Model B utilised the 3D beam element type B31 for the truss members and the truss element type T3D2 for the cable, while Model S used the four-noded doubly curved general-purpose shell element with reduced integration and finite membrane strains S4R for the truss members, and the eight-noded general purpose linear brick element with one integration point C3D8R [39] for the cable. Clearly, Model S is more sophisticated, but in the following discussion, it is assessed if Model B, which is much simpler and requires less computational time than Model S, can still provide suitably accurate results.

As described in Section 2.1, the trusses were fabricated in three parts, and featured two bolted connection assemblies on the bottom and top chords. When the truss is subjected to vertical loading, the bottom chord is under tension, rendering the flexibility of the connections important for the overall stiffness of the structure. To investigate this effect, firstly a numerical model of the connection alone was developed to determine its stiffness. The model was developed with 3D solid elements, eight-noded for the plate elements and stiffeners and ten-noded for the bolts, as shown in Fig. 10. Five elements were employed through the thickness of the plates. Given that only the initial stiffness of the connection was of interest, only the

elastic material properties of the steel components were employed. The connection was loaded under tensile static load and the deformed shape is shown in Fig. 10. The connection stiffness (k) was obtained by plotting the incremental load (kN) against the gap opening in the middle of the plates (mm) and was found to be equal to 590 kN/mm. Subsequently, having determined the connection stiffness (k), both models S and B were simulated with springs of axial stiffness 590 kN/mm and without springs in order to examine the effect of the stiffness of the connections on the overall response of the modelled trusses.

A mesh convergence study was carried out for both Model B and Model S to determine an adequately refined mesh size to provide accurate results within reasonable computational times. The boundary conditions for the models were applied so as to simulate accurately the experimental set-up. The structure was simply supported at its ends and the top chord joints were restrained laterally at the locations of the restraint cables. Vertical concentrated loads were applied to the bottom chords at the locations of the loading jacks. In line with previous studies [7], the loads in Model S were applied to the lower part of the web at the web-corner junction. The material properties of the steel tube and the prestressing cable measured in [8, 35] and reported in Table 2 herein were incorporated into the finite element models. For both the truss members and the cable, an elastic-perfectly plastic material model with the von Mises yield criterion and isotropic hardening was employed. For the shell and brick elements, true stress and logarithmic plastic strains were input into ABAQUS, while for the beam and truss elements, the engineering stress and strain properties were employed.

All structures contain initial geometric imperfections that can affect significantly their structural performance. In line with previous studies [7, 9-10] geometric imperfections were incorporated into the numerical simulations in the form of the mode shapes extracted from a linear eigenvalue buckling analysis, with suitable imperfection amplitudes determined through an imperfection sensitivity analysis. Both in-plane and out-of-plane failure modes were experimentally observed. Therefore, in order to accurately capture the test response, mode shapes for both of these cases – in-plane and out-of-plane, typical examples of which are shown in Fig. 11, were incorporated as imperfections in the nonlinear analyses.

Ten combinations of varying in-plane and out-of-plane geometric imperfection magnitudes, expressed as a function of the relevant truss element length L, were investigated. In order to examine the accuracy of the numerical models, the full load-displacement response was tracked, and the numerical to experimental ratios of the initial stiffness ($k_{initial,FE}/k_{initial,Exp}$), ultimate load ($F_{u,FE}/F_{u,Exp}$) and displacement at ultimate load ($\delta_{u,FE}/\delta_{u,Exp}$) were considered. Table 5 presents the results of the imperfection sensitivity analysis for Model S with springs for the four tested trusses (T1, T2, T3 and T4). It can be observed that while the ultimate load and the initial stiffness were generally well predicted for all the assumed imperfection amplitudes, the predicted vertical mid-span displacement at failure is more sensitive to the imperfection amplitude. Overall it was concluded that a model with an out-of-plane imperfection amplitude of L/750 and in-plane imperfection magnitude of L/1500 achieves very good agreement with the test results, with $F_{u,FE}/F_{u,Exp}$ and $k_{initial,FE}/k_{initial,Exp}$ equal to 0.98 and 1.02 respectively. Similar observations were also made for Model S without springs and Model

B with/without springs. Therefore, these imperfection amplitudes, along with the buckling modes shown in Fig. 11, were used in the models presented in Sections 3.2 (i.e. the validation study) and 3.3 (i.e. the parametric studies).

The residual stresses present in the studied members were found to be of very low magnitude [7-10] and were therefore not explicitly modelled. The Riks algorithm [40] was employed for the solution of the nonlinear analysis accounting for both material and geometric nonlinearities.

3.2 Model validation

The measured total load-mid-span displacement from the tests on Truss 1-Truss 4 are compared in Figs. 12(a)–12(d) with their respective FE predictions from Model B without the spring elements and Model S with the spring elements (i.e. the two extreme cases in terms of accuracy) at the bottom chord connections. As anticipated, Model B without springs over-predicts the stiffness of the system, whereas Model S with springs that account accurately for the actual stiffness of the joints leads to a more flexible response closer to the experimental observations. The deformed shapes for Model S with springs are compared with the test failure modes in Fig. 13, while the corresponding total load-mid-span deflection behaviour is summarised in Fig. 14, where accurate replication of the initial stiffness, ultimate load and general form of the load-deformation histories observed in the tests can be seen. Similar comparisons are made for Model B without springs in Fig. 15, where satisfactory agreement between the test and FE model results may be seen. Given the lower computational effort required for Model B, the possibility of its application in the subsequent parametric studies has been examined. To this end, a comparison between Model S with springs, which was shown to give the best agreement with the test results, and Model B without springs, which is most computationally efficient, was performed.

The comparison was based on the gains in strength and the corresponding reduction of the mid-span displacement (δ_u) at failure load (F_u) owing to prestress. The gains in strength were evaluated by normalising the ultimate load of the prestressed trusses (i.e. Trusses 2, 3 and 4) by the ultimate load of the bare truss (i.e. Truss 1). Similarly, the reduction in mid-span displacement at failure load was assessed by normalising the mid-span displacement of the models with $0.5P_{opt}$ and P_{opt} prestress (i.e. Truss 3 or 4) with the respective displacement of the model with nominal prestress P_{nom} (i.e. Truss 2). The results of the comparison are shown in Table 6. Note that B and S in the subscripts stand for Model B with no springs and Model S with springs respectively, while 1 and 2 refer the truss number. The ratio of the gains in strength from Model S and Model B was found to be equal to 1.01 while that of the reduction in mid-span displacement at failure was found to be equal to 1.07. It can be concluded that although Model B without springs overestimates the stiffness of the structure, it is capable of safely evaluating the gains in strength and the reduction in mid-span displacement at failure owing to the application of prestress. The aforementioned simplified model is therefore considered acceptable for the parametric studies in Section 3.3; this model is also reflective of that typically employed by practicing engineers.

3.3 Parametric studies

Following validation of the numerical models against the test results, an extensive parametric study was conducted in order to investigate the effect of key parameters including (1) prestress level, (2) material grade and (3) cross-section size of the chord elements on the structural response of prestressed steel trusses for a wide range of structural configurations likely to occur in practice.

The first parameter investigated was the level of the applied prestress and this was assessed by examining the arched truss considered previously for increasing prestress levels. The results are presented in normalised form in Fig. 16, where the total vertical load for all the studied cases has been normalised by the total vertical load at failure for the bare truss with no cable. The ultimate load may be seen to increase with the initial prestress level, whereas there is a corresponding reduction in the displacement at failure. For prestress forces higher than the P_{opt} value, no further benefit in terms of gains in strength or reduction of mid-span displacement at failure arise.

The second considered parameter was the steel grade of the truss members. The structural response of five trusses comprising elements in five readily available steel grades (S235, S275, S355, S460 and S690) was investigated. The same truss configuration and cross-section sizes from the validated FE model were employed. For the non-linear static analysis, the material stress-strain behaviour was assumed to be elastic-perfectly plastic, reflecting the presence of an extended yield plateau for hot-finished materials of all grades [41]. The results are presented in Fig. 17, where the loads are normalised by the respective failure loads of the bare trusses and plotted against the mid-span displacements. As can be seen, the introduction of prestress in trusses of various steel grades increases the failure load and reduces the mid-span displacement at failure. The gains in strength and reduction in mid-span displacement at failure are most significant when there is a large difference between the yield stress of the tube and of the prestressed cable (i.e. for mild steel structures) but are still considerable for high strength steel structures.

The final investigated parameter was the employed cross-section sizes for the top (A_{top}) and bottom chords (A_{bot}) and was assessed in terms of the ratio of their cross-sectional areas. Four prestress levels (i.e. no cable, P_{nom}, $0.5P_{opt}$, P_{opt}) were studied for the following five cases – Case (a): Top chord SHS 70×70×7, bottom chord SHS 40×40×4, A_{top}/A_{bot} = 2.80, Case (b): Top chord SHS 80×80×8, bottom chord SHS 50×50×5, A_{top}/A_{bot} = 2.56, Case (c): Top chord SHS 70×70×7, bottom chord SHS 50×50×5, A_{top}/A_{bot} =1 .79, Case (d): Top chord SHS 60×60×6, bottom chord SHS 50×50×5, A_{top}/A_{bot} = 1.44 and Case (e): Top chord SHS 70×70×7, bottom chord SHS 60×60×6, A_{top}/A_{bot} = 1.25.

The gains in strength and reduction in mid-span displacement at failure, together with the corresponding failure modes, are presented in Table 7, leading to the following observations: in Cases (a) and (b) with the largest A_{top}/A_{bot} ratios, the introduction of prestress increases the ultimate load. In Case (a), no significant strength gains appeared for varying prestress levels, whereas in Case (b), the large section of the top chord delayed buckling and the truss failed

due to yielding of the tensile bottom chord, leading to more prominent strength gains for increasing prestress levels. Case (c), which had an intermediate A_{top}/A_{bot} ratio, presented increasing gains (both in strength and in reduction of the mid-span displacement at failure) for increasing prestress. Note that the test specimens described earlier correspond to Case (c). Cases (d) and (e), which had the lowest A_{top}/A_{bot} ratios, did not present any gains following the introduction of prestress. This is because the trusses failed prematurely due to out-of-plane buckling of the top chord, preventing the benefits of prestress from emerging. Hence it can be stated that the truss design significantly affects the performance benefits that can be achieved through the application of prestress. For optimal performance, failure due to yielding of the tension chord should occur prior to the buckling of the compression chord, thus ensuring a ductile failure mode and increasing the beneficial effect of prestressing.

4. Design Recommendations

Having investigated the structural response of prestressed trusses, design guidance is presented in this section, with a focus simply-supported trusses employing tubular members. A flow chart of the design process is given in Fig. 18, and is explained hereafter.

As a first step, the overall geometry of the truss (i.e. span, depth, configuration of diagonals and curvature of the bottom and top chord) should be chosen. As in conventional truss design, the final choice is a compromise between aesthetics, economy, weight, fabrication cost and so on, and is usually the result of a number of iterations.

The second step involves the determination of the relevant actions for both the Ultimate Limit State (ULS) and Serviceability Limit State (SLS). The various relevant load cases and combinations should be established and compared, from which the most critical, in both the gravity and uplift directions, should be identified. Loads are assumed herein to act only at the joint locations and hence only truss action (i.e. pure tension or pure compression in the truss members) is considered.

The next step is to determine the cross-section sizes of the truss members. The procedure begins with the design of the bottom chord. With the assumption that the truss behaves approximately as a simply-supported beam, subjected to either uniform gravity or uplift loading, the design mid-span bending moment and hence the design tensile or compressive force in the bottom chord, $N_{Ed,bot,t}$ (or $N_{Ed,bot,c}$) can be approximated.

The selection of the yield strengths (f_{cy} and f_{ty}) and cross-sectional areas (A_c and $A_{t,bot}$) of the cable and steel tube at the bottom chord, as well as the level of prestress P_i, should be made on the basis of satisfying Eqs (4) and (5), under gravity and uplift loading, respectively. It should be noted that P_i should not be larger than the minimum of the optimum prestress (P_{opt}) and the yield loads of the cable ($A_c f_{cy}/\gamma_{M0}$) and the tube ($A_{t,bot} f_{ty}/\gamma_{M0}$).

$$N_{Ed,bot,t} \leq N_{pl,Rd,bot} \tag{4}$$

$$N_{Ed,bot,c} \leq N_{b,Rd,bot} \tag{5}$$

The design plastic resistance of the cable-in-tube bottom chord $N_{pl,Rd,bot}$ is determined from Eq. (6), assuming that failure occurs when the steel tube yields, even though the system may resist further loads due to the contribution of the cable.

$$N_{pl,Rd,bot} = \frac{1}{\gamma_{M0}}\left(A_{t,bot}f_{ty} + P_i\right)\left(1 + \frac{E_c A_c}{E_t A_{t,bot}}\right) \tag{6}$$

where E_c and E_t are the Young's moduli of the cable and the steel tube, respectively, and γ_{M0} is the partial factor for resistance of cross-sections with a recommended value of 1.0.

The design buckling resistance of the bottom chord member $N_{b,Rd,bot}$ is obtained from the modified Perry-Robertson approach proposed by Gosaye et al. 2016 [32] and Wang et al. [35], in conjunction with the codified column buckling curves in EN 1993-1-1 [38]. This is presented in Eq. (7) as the product of the buckling reduction factor χ_p and the yield load of the steel tube $N_{pl} = A_{t,bot}f_{ty}$.

$$N_{b,Rd,bot} = \frac{\chi_p N_{pl}}{\gamma_{M1}} \tag{7}$$

where χ_p is given by:

$$\chi_p = \frac{1 - P_i/N_{pl}}{\alpha_k\left[\phi_p + \sqrt{\phi_p^2 - \left(1 - P_i/N_{pl}\right)\bar{\lambda}^2/\alpha_k}\right]} \tag{8}$$

with ϕ_p defined as:

$$\phi_p = \frac{\left(1 - P_i/N_{pl}\right)\bar{\lambda}^2 + \alpha_k + \alpha(\bar{\lambda} - 0.2)}{2\alpha_k} \tag{9}$$

In Eqs (8) and (9), $\bar{\lambda}$ is the member slenderness defined as $\bar{\lambda} = \sqrt{N_{pl}/N_{cr}}$, where N_{pl} is the yield load and N_{cr} is the elastic buckling load of the tubular member, α is the imperfection factor and $\alpha_k = K_t/(K_c + K_t)$ is the ratio of the axial stiffness of the tube to that of the cable-in-tube-system, where K_c and K_t are the axial stiffness of the cable and the tube (A_cE_c/L and A_tE_t/L), respectively.

The imperfection factor α is selected from EN 1993-1-1 [38], but on the basis of an effective yield strength of the tube, defined as $f_{ty,eff} = f_{ty}\text{-}P_i/A_{t,bot}$. It was recommended in [35] that buckling curve a with $\alpha = 0.21$ and buckling curve a_0 with $\alpha = 0.13$ should be used for hot-finished tubular members with $f_{ty,eff} < 460$ N/mm^2 and $f_{ty,eff} \geq 460$ N/mm^2, respectively. This is

because prestressed columns effectively have a reduced yield strength, due to the prestressing, when loaded in compression; columns with a reduced yield strength are more sensitive to geometric imperfections [2] and contain residual stresses that are a higher proportion of the yield strength, both of which impinge on the column buckling resistance.

The top chord should be designed to resist the maximum tensile and compressive design loads ($N_{Ed,top,t}$ and $N_{Ed,top,c}$), which correspond to uplift and gravity loading, respectively. The tensile and compressive design criteria are shown in Eqs (10) and (11), respectively. Note that, in order to have a ductile failure mode under gravity loading, buckling of the compressed top chord (both in-plane and out-of-plane) should occur after yielding of the bottom chord in tension (i.e. $\frac{N_{Ed,top,c}}{N_{b,Rd,top}} \leq \frac{N_{Ed,bot,c}}{N_{pl,Rd,bot}}$)

$$N_{Ed,top,t} \leq N_{pl,Rd,top} = A_{top} f_{ty} / \gamma_{M0} \tag{10}$$

$$N_{Ed,top,c} < N_{b,Rd,top} \tag{11}$$

where A_{top} is the cross-sectional area of the top chord member, and $N_{b,Rd,top}$ is the design buckling resistance of the top chord, calculated according to the design rules set out in EN 1993-1-1 [38]. Note that the strength and stiffness of the lateral restraints against out-of-plane buckling should also be verified [38], but the requirements remain the same as for other systems.

Finally, the cross-sectional area of the diagonals A_{diag} can then be evaluated from Eqs (12) and (13), to resist the tensile and compressive design forces in the these members ($N_{Ed,diag,t}$ and $N_{Ed,diag,c}$).

$$N_{Ed,diag,t} \leq N_{pl,Rd,diag} = A_{diag} f_{ty} / \gamma_{M0} \tag{12}$$

$$N_{Ed,diag,c} < N_{b,Rd,diag} \tag{13}$$

where $N_{b,Rd,diag}$ is the buckling resistance of the diagonal members, as defined in EN 1993-1-1 [38].

Applying the proposed design procedure to the tested trusses, using the measured geometric and material properties and with partial safety factors set to unity, results in load carrying predictions for the four trusses within 3.6% of their experimental failure loads.

5. Conclusions

The structural response of prestressed steel trusses has been investigated herein through experimentation and numerical analysis. The test specimens included four 11 m span arched trusses comprising S460 hot-finished square hollow sections. A purpose-built rig was designed in order to apply vertical downward loading to the trusses and obtain the structural response up to failure. It was shown that inclusion of prestressing cables within the bottom chords of the

trusses can result in substantial increases in structural resistance (up to 40% for a 3% increase in self-weight for the tested specimens), while prestressing of the cables delays yielding of the bottom chord and extends the elastic range of the system, thus reducing deformations at failure (up to around 50% for the tested specimens). Finite element models were generated and validated against the test results. Based on the validated FE models, parametric studies were performed, which showed that the application of prestress can be beneficial for trusses of several structural configurations, provided that the truss members are suitably proportioned. To this end, simplified design guidance has been established and verified against the experimental results. Overall it can be concluded that the use of prestress cables housed within the bottom chords of tubular structures can offer substantial improvements in structural performance with very modest increases in self-weight, making this structural system well suited to long-span applications.

Acknowledgements

The research leading to these results has received funding from the Research Fund for Coal and Steel (RFCS) under grant agreement No. RFSR CT 2012-00028.

References

[1] EN1993-1-12., 2007. Eurocode 3: Design of steel structures - part 1-12: Additional rules for the extension of EN 1993 up to steel grades S700, European committee for standardization (CEN).

[2] Johansson, B., 2005. 5.3 Buckling Resistance of Structures of High Strength Steel. *Use and Application of High-performance Steels for Steel Structures*, *8*, pp.120.

[3] Rasmussen, K.J.R. and Hancock, G.J., 1995. Tests of high strength steel columns. *Journal of Constructional Steel Research*, *34*(1), pp.27-52.

[4] Kim, D.K., Lee, C.H., Han, K.H., Kim, J.H., Lee, S.E. and Sim, H.B., 2014. Strength and residual stress evaluation of stub columns fabricated from 800MPa high-strength steel. *Journal of Constructional Steel Research*, *102*, pp.111-120.

[5] Beg, D. and Hladnik, L., 1996. Slenderness limit of class 3 I cross-sections made of high strength steel. *Journal of Constructional Steel Research*, *38*(3), pp.201-217.

[6] Rasmussen, K.J.R. and Hancock, G.J., 1992. Plate slenderness limits for high strength steel sections. *Journal of Constructional Steel Research*, *23*(1), pp.73-96.

[7] Wang, J., Afshan, S., Gkantou, M., Theofanous, M., Baniotopoulos, C. and Gardner, L., 2016. Flexural behaviour of hot-finished high strength steel square and rectangular hollow sections. *Journal of Constructional Steel Research*, *121*, pp.97-109.

[8] Wang J., Afshan S., Schillo N., Theofanous M., Feldmann M., and Gardner L. Material properties and local buckling behaviour of high strength steel square and rectangular hollow sections. *Engineering Structures*, *130*, pp.297-315.

[9] Gkantou M., Theofanous M., Wang J., Baniotopoulos C., and Gardner L. Behaviour and Design of high strength steel cross-sections under combined loading. *Proceedings of the Institution of Civil Engineers, 170*(11), pp.841-854.

[10] Gkantou M., Theofanous M., Antoniou N., Baniotopoulos C. Compressive behaviour of high strength steel cross-sections. *Proceedings of the Institution of Civil Engineers, 170*(11), pp.813-824.

[11] Magnel, G., 1950. Prestressed steel structures. *The Structural Engineer*, *28*(11), pp.285-295.

[12] Belenja, E.I., 1977. Prestressed load-bearing metal structures. Mir Publishers, Moscow.

[13] Ellen, P.E., Elspan International Limited, 1987. *Post-tensioned steel structure*. U.S. Patent 4,676,045.

[14] Hancock, G.J., Olsen, C.J. and Key, P.W., 1988. *Structural behaviour of a stressed arch structural system*. University of Sydney, School of Civil and Mining Engineering.

[15] Clarke, M.J. and Hancock, G.J., 1991. Finite-element nonlinear analysis of stressed-arch frames. *Journal of Structural Engineering, ASCE*, *117*(10), pp.2819-2837.

[16] Clarke, M.J. and Hancock, G.J., 1994. Simple design procedure for the cold-formed tubular top chord of stressed-arch frames. *Engineering Structures*, *16*(5), pp.377-385.

[17] Clarke, M.J. and Hancock, G.J., 1995. Tests and nonlinear analyses of small-scale stressed-arch frames. *Journal of Structural Engineering, ASCE*, *121*(2), pp.187-200.

[18] Madrazo-Aguirre, F., Ruiz-Teran, A.M. and Wadee, M.A., 2015. Dynamic behaviour of steel–concrete composite under-deck cable-stayed bridges under the action of moving loads. *Engineering Structures*, *103*, pp.260-274.

[19] Belletti, B. and Gasperi, A., 2010. Behavior of prestressed steel beams. *Journal of Structural Engineering*, *136*(9), pp.1131-1139.

[20] Hadjipantelis, N., Gardner, L. and Wadee, M. Ahmer. (2018). Prestressed cold-formed steel beams: Concept and mechanical behaviour. *Engineering Structures*. *172*, 1057-1072.

[21] Hadjipantelis, N., Gardner, L. and Wadee, M. Ahmer. (submitted). Finite element modelling of prestressed cold-formed steel beams. *Journal of Structural Engineering, ASCE*.

[22] Saito, D. and Wadee, M.A., 2010. Optimal prestressing and configuration of stayed columns. *Proceedings of the Institution of Civil Engineers-Structures and Buildings*, *163*(5), pp.343-355.

[23] Wadee, M.A., Gardner, L. and Osofero, A.I., 2013. Design of prestressed stayed columns. *Journal of Constructional Steel Research*, *80*, pp.287-298.

[24] Ayyub, B.M., Ibrahim, A. and Schelling, D., 1990. Posttensioned trusses: Analysis and design. *Journal of Structural Engineering, ASCE*, *116*(6), pp.1491-1506.

[25] Ayyub, B.M. and Ibrahim, A., 1990. Posttensioned trusses: Reliability and redundancy. *Journal of Structural Engineering, ASCE*, *116*(6), pp.1507-1521.

[26] Li, H. and Schmidt, L.C., 1997. Posttensioned and Shaped Hypar Space Trusses. *Journal of Structural Engineering, ASCE*, *123*(2), pp.130-137.

[27] Han, K.B. and Park, S.K., 2005. Parametric study of truss bridges by the post-tensioning method. *Canadian Journal of Civil Engineering*, *32*(2), pp.420-429.

[28] Bourne, S., 2013. Prestressing: recovery of the lost art. *Struct Eng*, *91*(2), pp.12-22.

[29] Lee, K., Huque, Z. and Han, S., 2014. Analysis of stabilizing process for stress-erection of Strarch frame. *Engineering Structures*, *59*, pp.49-67.

[30] Garlock, M., Sause, R. and Ricles, J., 2004. Design and behaviour of post-tensioned steel moment frames. In *Proceedings of the 13th World Conference on Earthquake Engineering*.

[31] Ellen, M.E., Gosaye, J., Gardner, L. and Wadee, M.A., 2012. Design and construction of long-span post-tensioned tubular steel structures. *Tubular structures XIV*, pp.687-693.

[32] Gosaye, J., Gardner, L., Wadee, M.A. and Ellen, M.E., 2016, February. Compressive behaviour and design of prestressed steel elements. *Structures 5*, pp.76-87.

[33] Gosaye, J., Gardner, L., Wadee, M.A. and Ellen, M.E., 2014. Tensile performance of prestressed steel elements. *Engineering Structures*, *79*, pp.234-243.

[34] Creators of super powerful structures. (2016) Available from: http://www.s-squared.com.au/home.aspx.

[35] Wang, J., Afshan, S. and Gardner, L., 2016. Axial behaviour of prestressed high strength steel tubular members. *Journal of Constructional Steel Research*, *133*, pp.547-563.

[36] BS 5896 (2010). High tensile steel wire and strand for the prestressing of concrete – Specification. British Standards Institution (BSI).

[37] EN 10210-2., 2006. Hot finished structural hollow sections of non-alloy and fine grain steels. Tolerances, dimensions and sectional properties, European committee for standardization (CEN).

[38] EN 1993-1-1., 2005. Eurocode 3: Design of steel structures – part 1-1: General rules and rules for buildings, European committee for standardization (CEN).

[39] Hibbitt, Karlsson, Sorensen Inc. ABAQUS., 2010, ABAQUS/Standard user's manual volumes I–III and ABAQUS CAE manual.Version 6.10. USA: Pawtucket.

[40] Riks, E., 1979. An incremental approach to the solution of snapping and buckling problems. *International Journal of Solids and Structures*, *15*(7), pp.529-551.

[41] Yun, X. and Gardner, L. (2017). Stress-strain curves for hot-rolled steels. *Journal of Constructional Steel Research*. *133*, pp.36-46.

Tables

Table 1: Average measured geometric dimensions of the truss elements.

Section	h (mm)	b (mm)	t (mm)	r_i (mm)
SHS 70×70×6.3	69.95	70.02	6.21	3.79
SHS 50×50×5	50.48	50.44	4.95	3.50
SHS 40×40×2.9	40.16	40.20	2.87	1.27

Table 2: Average measured material properties of the high strength steel tubular truss elements and prestressing cable.

Member	E (N/mm^2)	f_y (N/mm^2)	f_u (N/mm^2)	ε_u (%)	ε_f (%)
SHS 70×70×6.3	211805	531	752	12.3	26.3
SHS 50×50×5	210000	505	620	14.9	31.0
SHS 40×40×2.9	206100	512	683	14.0	30.0
Prestressing cable	130000	1703	1800	-	-

Table 3: Nominal and measured prestress loads.

Specimen	Nominal prestress force (kN)	Measured prestress force (kN)
Truss 1	0	0
Truss 2	5.0 (P_{nom})	5.9 (P_{nom})
Truss 3	94.5 ($0.5P_{opt}$)	80.8 ($0.43P_{opt}$)
Truss 4	189.0 (P_{opt})	149.9 ($0.79P_{opt}$)

Table 4: Measured ultimate loads (total of 5 point loads) and failure modes from truss tests.

Specimen	Failure mode	Yield load (kN)	Ultimate load (kN)
Truss 1	Yielding of bottom chord element	177.6	185.4
Truss 2	In-plane buckling of top chord element	210.6	258.0
Truss 3	Out-of-plane buckling of top chord element	241.2	243.2
Truss 4	In-plane buckling of top chord element	269.2	269.2

Table 5: Imperfection sensitivity study – summary for all trusses.

All trusses							
Imperfection magnitude		$F_{u,FE}/F_{u,Exp}$		$\delta_{u,FE}/\delta_{u,Exp}$ (only for L3)		$k_{initial,FE}/k_{initial,Exp}$ (only for L3)	
Out-of-plane	In-plane	MEAN	COV	MEAN	COV	MEAN	COV
L/1000	L/1000	0.99	0.041	1.02	0.176	1.02	0.043
L/2000	L/1000	1.01	0.041	1.15	0.180	1.02	0.043
L/1000	L/2000	1.00	0.053	1.03	0.175	1.02	0.043
L/1500	L/750	1.01	0.040	1.10	0.174	1.02	0.043
L/750	**L/1500**	**0.98**	**0.042**	**0.96**	**0.178**	**1.02**	**0.043**
L/1000	0	0.99	0.041	1.03	0.175	1.02	0.043
0	L/1000	1.04	0.047	1.32	0.236	1.02	0.043
L/2000	L/2000	1.02	0.041	1.15	0.181	1.02	0.043
L/750	L/750	0.98	0.044	0.96	0.185	1.02	0.043
L/1500	L/1500	1.01	0.041	1.10	0.176	1.02	0.043

Table 6: Gains in strength and reduction of the mid-span displacement at failure load - comparison between Model S with springs and Model B with no springs.

Specimen	Model S with springs				Model B with no springs				Model B / Model S	
	F_{uS} (kN)	δ_{uS} (mm)	F_{uS}/F_{uS1}	δ_{uS}/δ_{uS2}	F_{uB} (kN)	δ_{uB} (mm)	F_{uB}/F_{uB1}	δ_{uB}/δ_{uB2}	$(F_{uB}/F_{uB1})/(F_{uS}/F_{uS1})$	$(\delta_{uB}/\delta_{uB2})/(\delta_{uS}/\delta_{uS2})$
Truss 1	185.6	108.2	-	-	195.2	97.2	-	-	-	-
Truss 2	242.1	237.4	1.30	-	256.8	207.9	1.32	-	1.01	-
Truss 3	248.6	172.2	1.34	0.73	265.2	162.1	1.36	0.78	1.01	1.07
Truss 4	255.6	134.4	1.38	0.57	267.4	125.6	1.37	0.60	0.99	1.07
MEAN									1.01	1.07
COV									0.01	0.05

Table 7: Effect of chord section ratio (A_{top}/A_{bot}) on response of prestressed trusses.

	Prestress level	Gains - Strength	Reductions - Displacement	Failure mode
Case (a):	No cable	-	-	Y
Top chord 70×70×7	P_{nom}	67%	-	Y & OUT
Bottom chord 40×40×4	$0.5P_{opt}$	73%	22%	Y & OUT
A_{top}/A_{bot} =2.80	P_{opt}	76%	46%	Y & OUT
Case (b):	No cable	-	-	Y
Top chord 80×80×8	P_{nom}	47%	-	Y & OUT
Bottom chord 50×50×5	$0.5P_{opt}$	47%	15%	Y & OUT
A_{top}/A_{bot} =2.56	P_{opt}	49%	70%	Y & OUT
Case (c):	No cable	-	-	Y
Top chord 70×70×7	P_{nom}	21%	-	Y & OUT
Bottom chord 50×50×5	$0.5P_{opt}$	26%	38%	Y & OUT
A_{top}/A_{bot} =1.79	P_{opt}	28%	46%	Y & OUT
Case (d):	No cable	-	-	OUT
Top chord 60×60×6	P_{nom}	2%	-	OUT
Bottom chord 50×50×5	$0.5P_{opt}$	2%	0%	OUT
A_{top}/A_{bot} =1.44	P_{opt}	2%	0%	OUT
Case (e):	No cable	-	-	OUT
Top chord 70×70×7	P_{nom}	0%	-	OUT
Bottom chord 60×60×6	$0.5P_{opt}$	0%	0%	OUT
A_{top}/A_{bot} =1.25	P_{opt}	0%	0%	OUT

Y=Yielding of the tensile bottom chord
OUT= Out-of-plane buckling of the compressive top chord

Figures

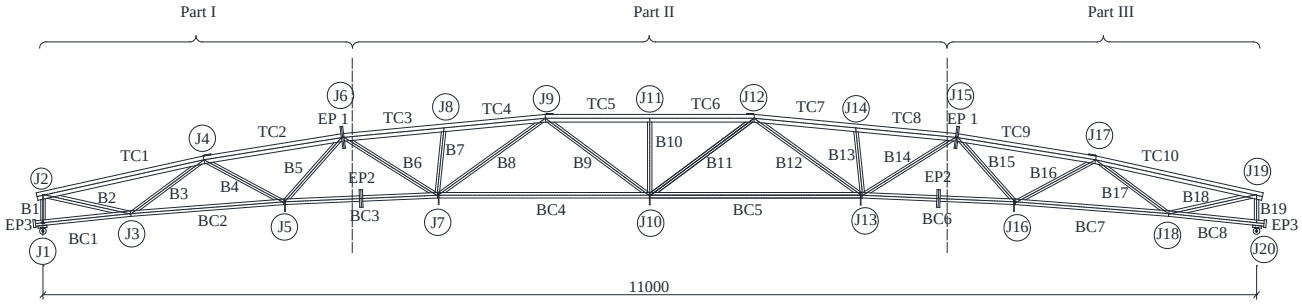

Coordinates of joints J1-J20:

J1 (0, 0)	J11 (5500, 950)
J2 (0, 250)	J12 (6447, 950)
J3 (795, 85)	J13 (7425, 250)
J4 (1459, 573)	J14 (7365, 864)
J5 (2183, 190)	J15 (8283, 777)
J6 (2717, 777)	J16 (8817, 190)
J7 (3575, 250)	J17 (9541, 573)
J8 (3635, 864)	J18 (10205, 85)
J9 (4553, 950)	J19 (11000, 250)
J10 (5500, 250)	J20 (11000, 0)

All dimensions are in millimetres (mm)

Members	Element label	Steel grade	Section sizes
Top chord	TC1-TC10	S460	SHS 70×70×6.3
Bottom chord	BC1-BC8	S460	SHS 50×50×5
Verticals/diagonals	B1-B18	S460	SHS 40×40×2.9
End-plates	EP1	S355	SHS 200×200×10
	EP2	S355	SHS 160×160×15
	EP3	S355	SHS 70×70×20

Fig.1: Schematic drawing of the arched truss test specimens.

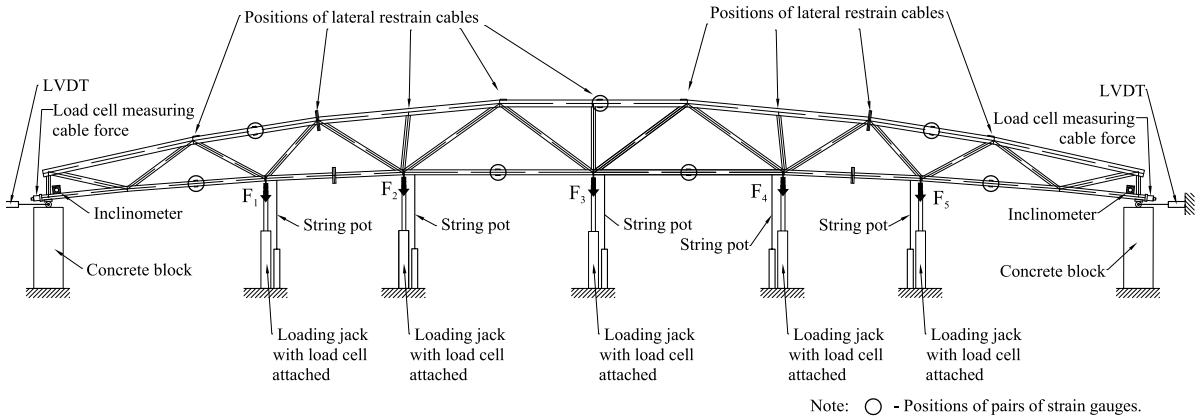

(a) Schematic diagram

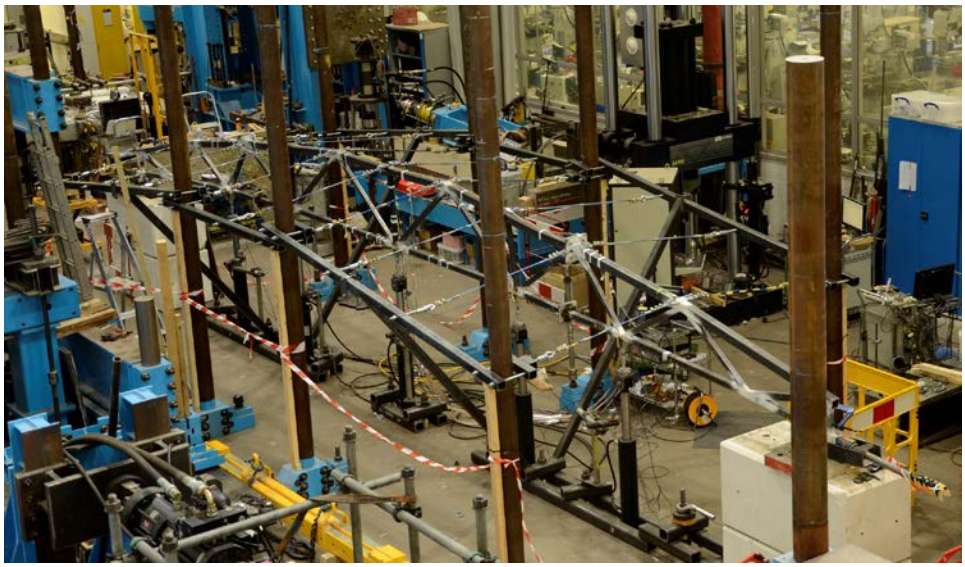

(b) Test set-up

Fig. 2: Test rig set-up and instrumentation.

Fig. 3: Detail of the loading jack to truss connection via steel plate.

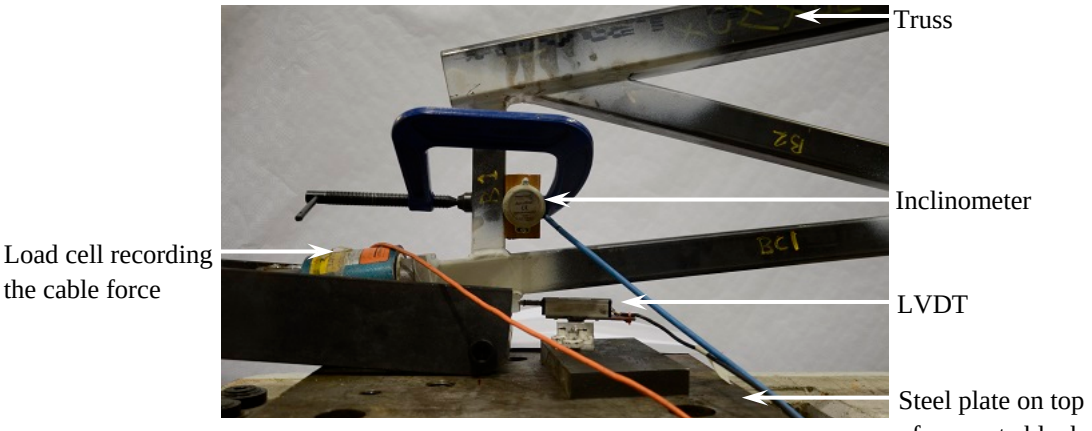

Fig. 4: Detail of truss end support condition.

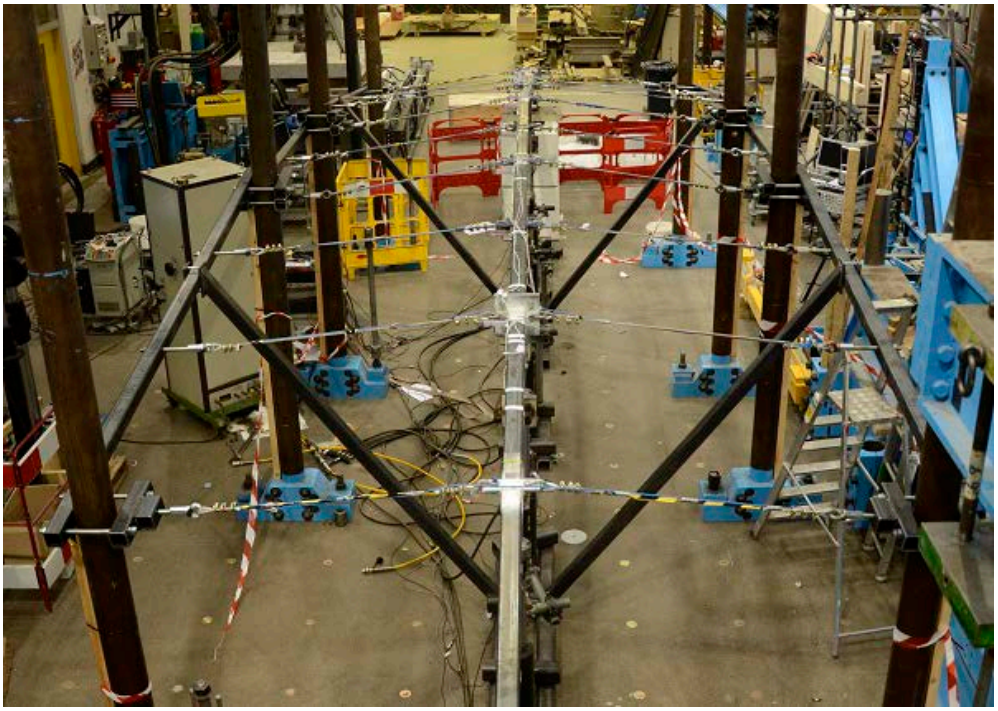

(a) Overall scheme

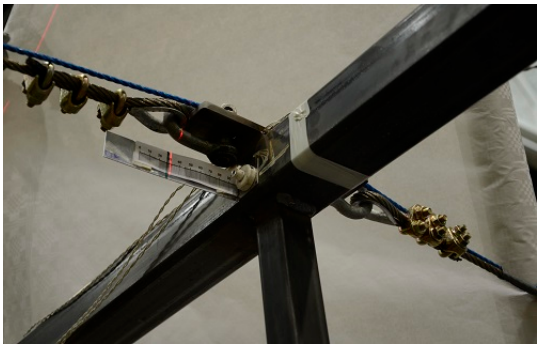

(b) Cable to truss connection

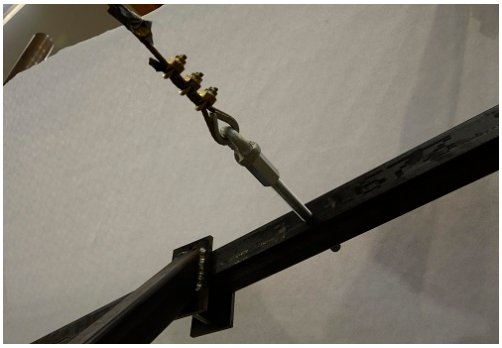

(c) Cable to test rig connection

Fig. 5: Details of lateral restraint connections.

Fig. 6: Prestressing of cable

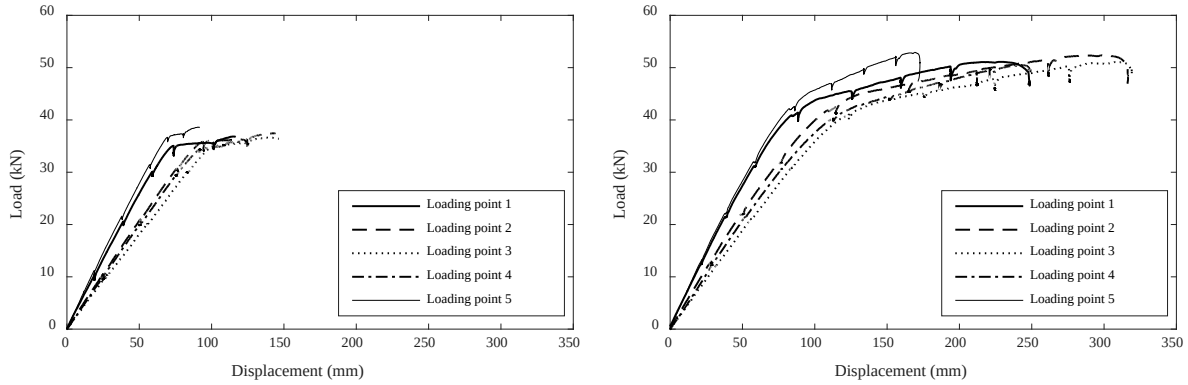

(a) Truss 1 (control specimen)

(b) Truss 2 (P_{nom})

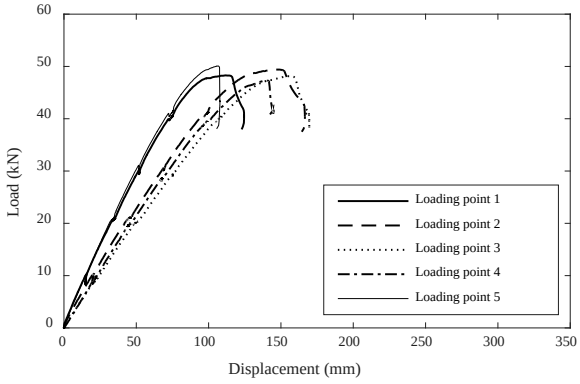

(c) Truss 3 ($0.5P_{opt}$)

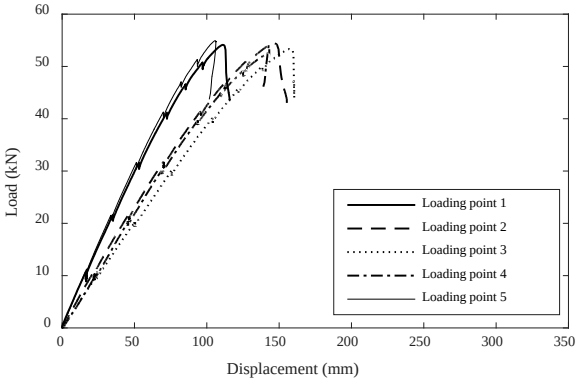

(d) Truss 4 (P_{opt})

Fig. 7: Curves of load versus vertical displacement at the five loading points.

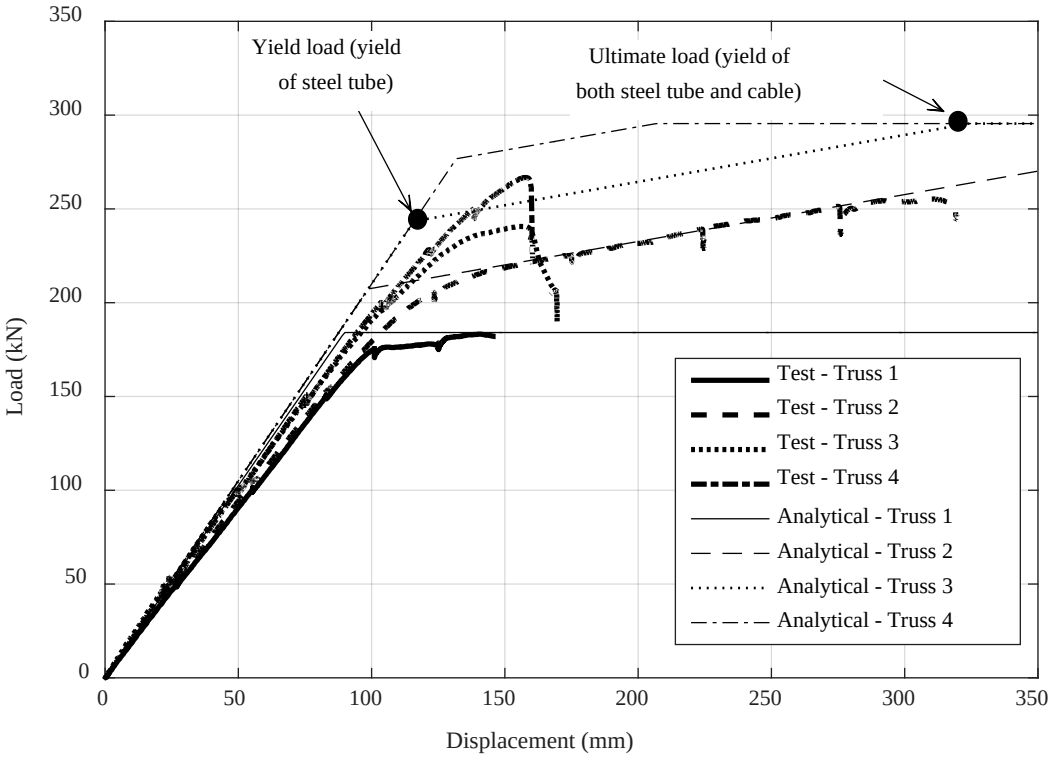

Fig. 8: Test and analytical total load versus mid-span vertical displacement curves.

(a) In-plane failure mode observed in Truss 2 and 4 tests

(b) Out-of-plane buckling of top chord of Truss 3

Fig. 9: Observed experimental failure modes.

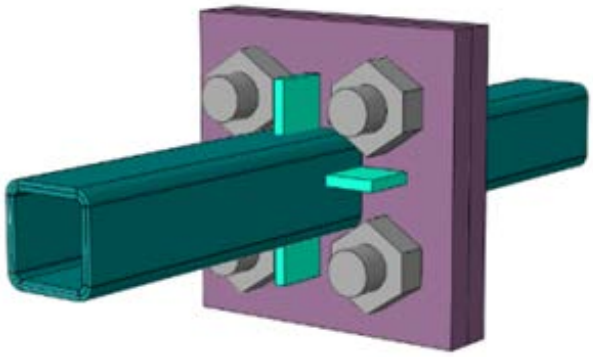

(a) Finite element model

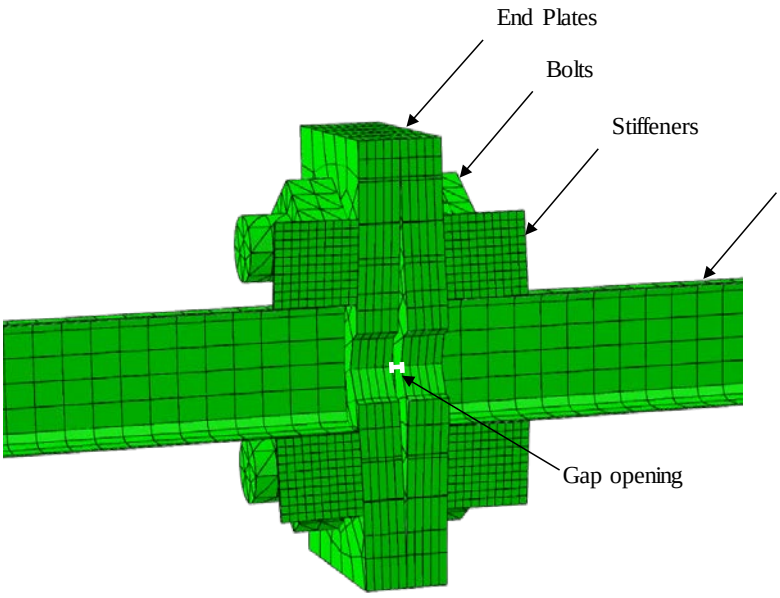

(b) Deformed shape illustrating the gap opening

Fig. 10: Model of the connection assembly in bottom chord.

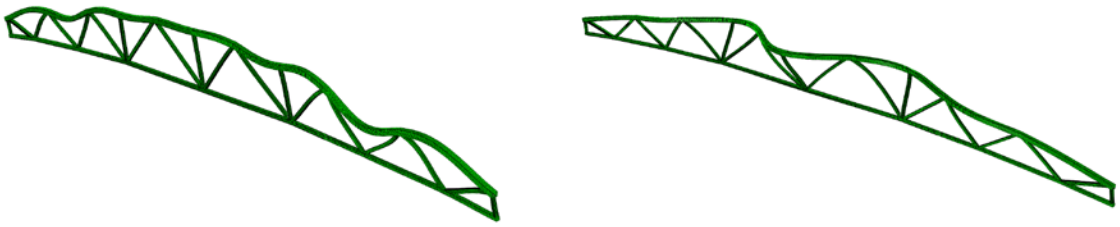

(a) In-plane mode (b) Out-of-plane mode

Fig. 11: Elastic buckling modes.

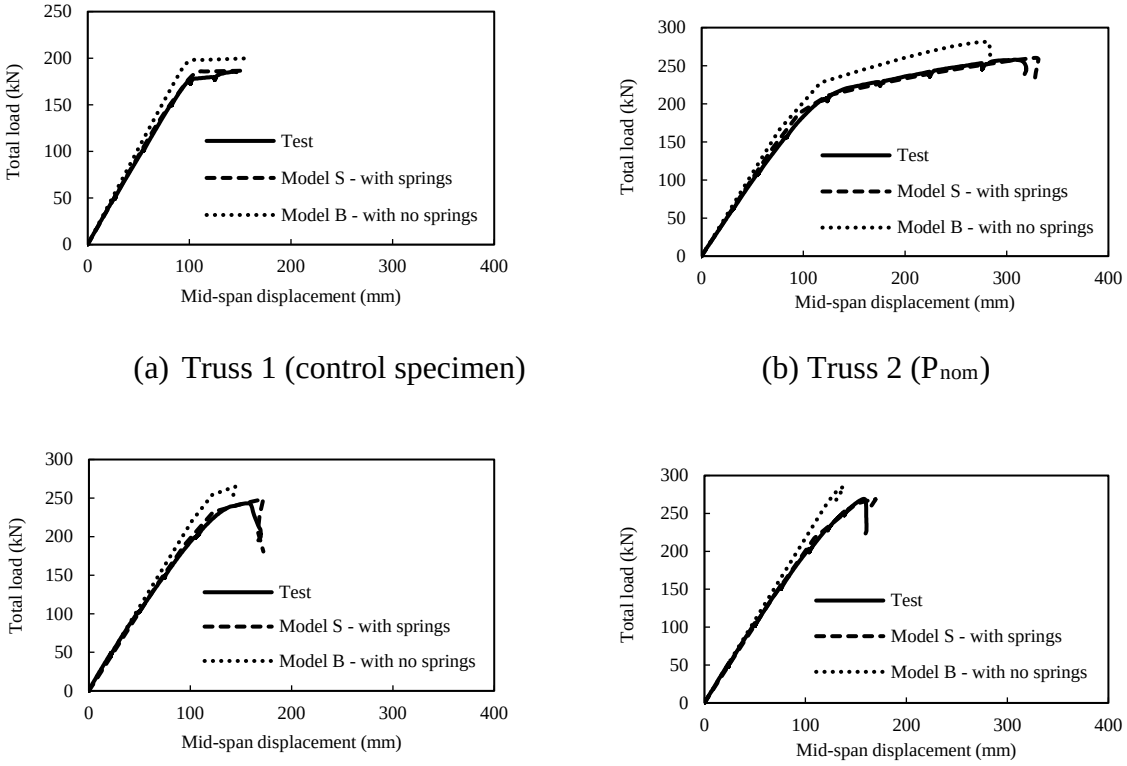

(a) Truss 1 (control specimen) (b) Truss 2 (P_{nom})

(c) Truss 3 ($0.5P_{opt}$) (d) Truss 4 (P_{opt})

Fig. 12: Comparison between test and FE total load versus mid-span displacement curves.

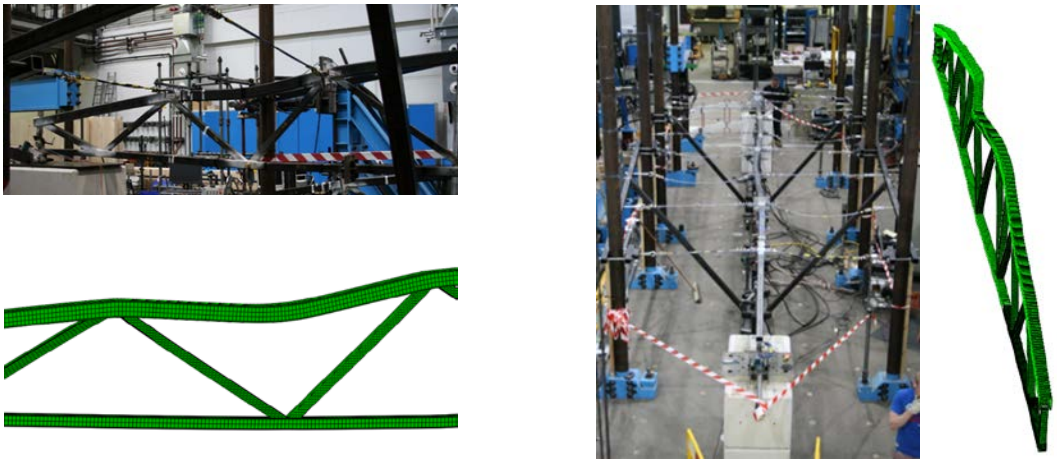

(a) In-plane failure mode (b) Out-of-plane failure mode

Fig. 13: Replication of experimentally observed failure modes by numerical models.

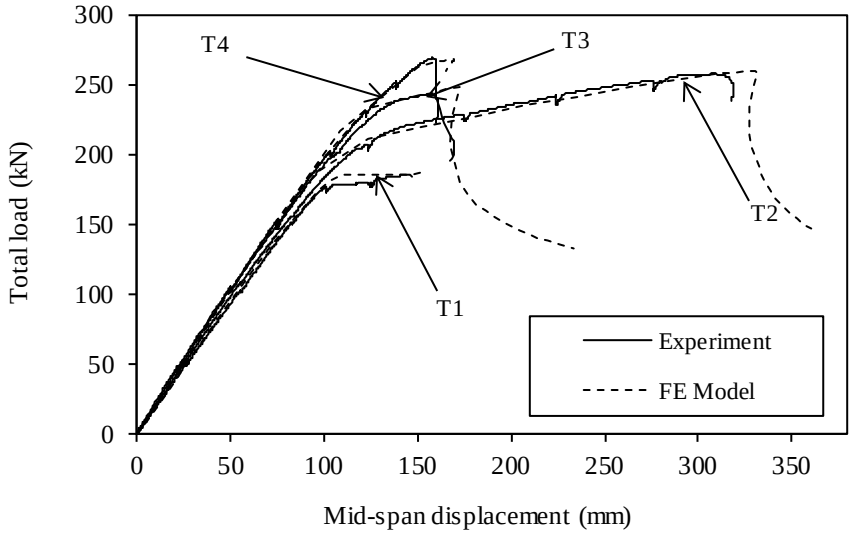

Fig. 14: Comparison between experimental and FE (Model S with springs) load-displacement curves.

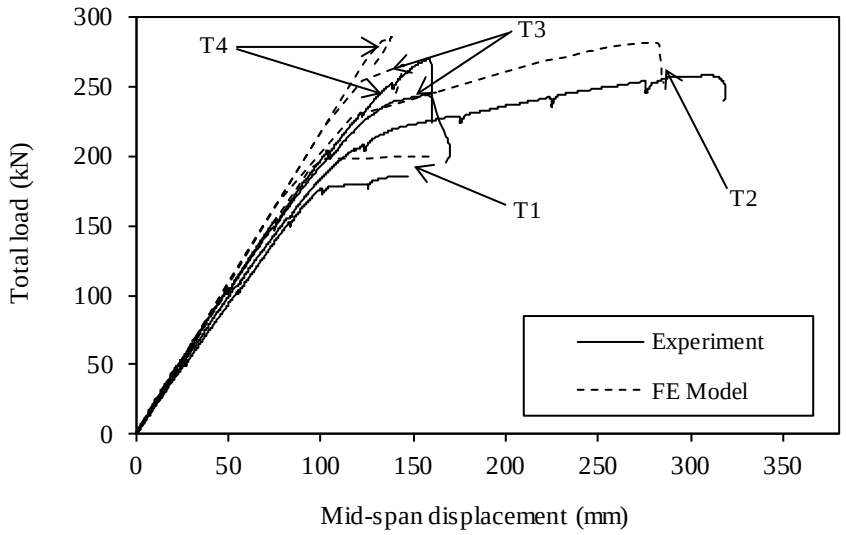

Fig. 15: Comparison between experimental and FE (Model B with no springs) load-displacement curves.

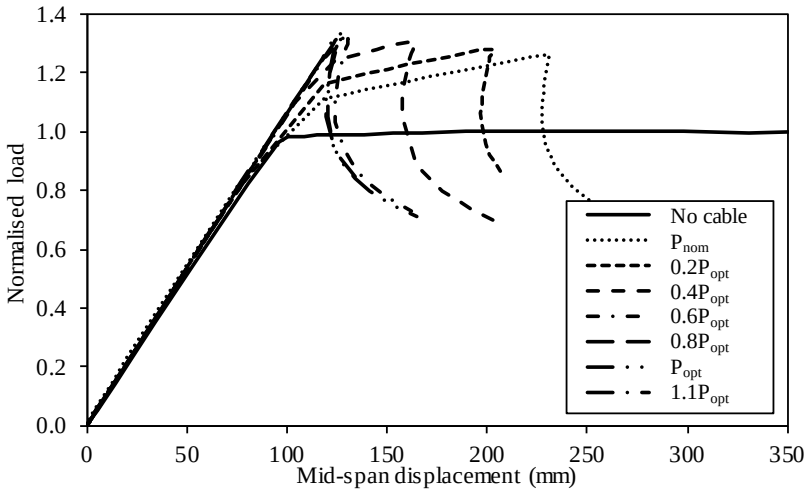

Fig. 16: Normalised load versus mid-span displacement of trusses for various levels of applied prestress.

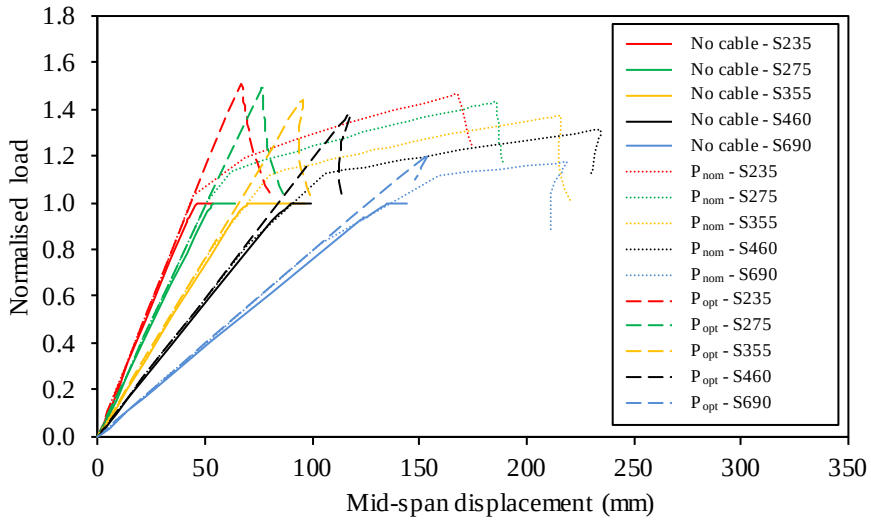

Fig. 17: Normalised load versus mid-span displacement curves for trusses of various steel grades.

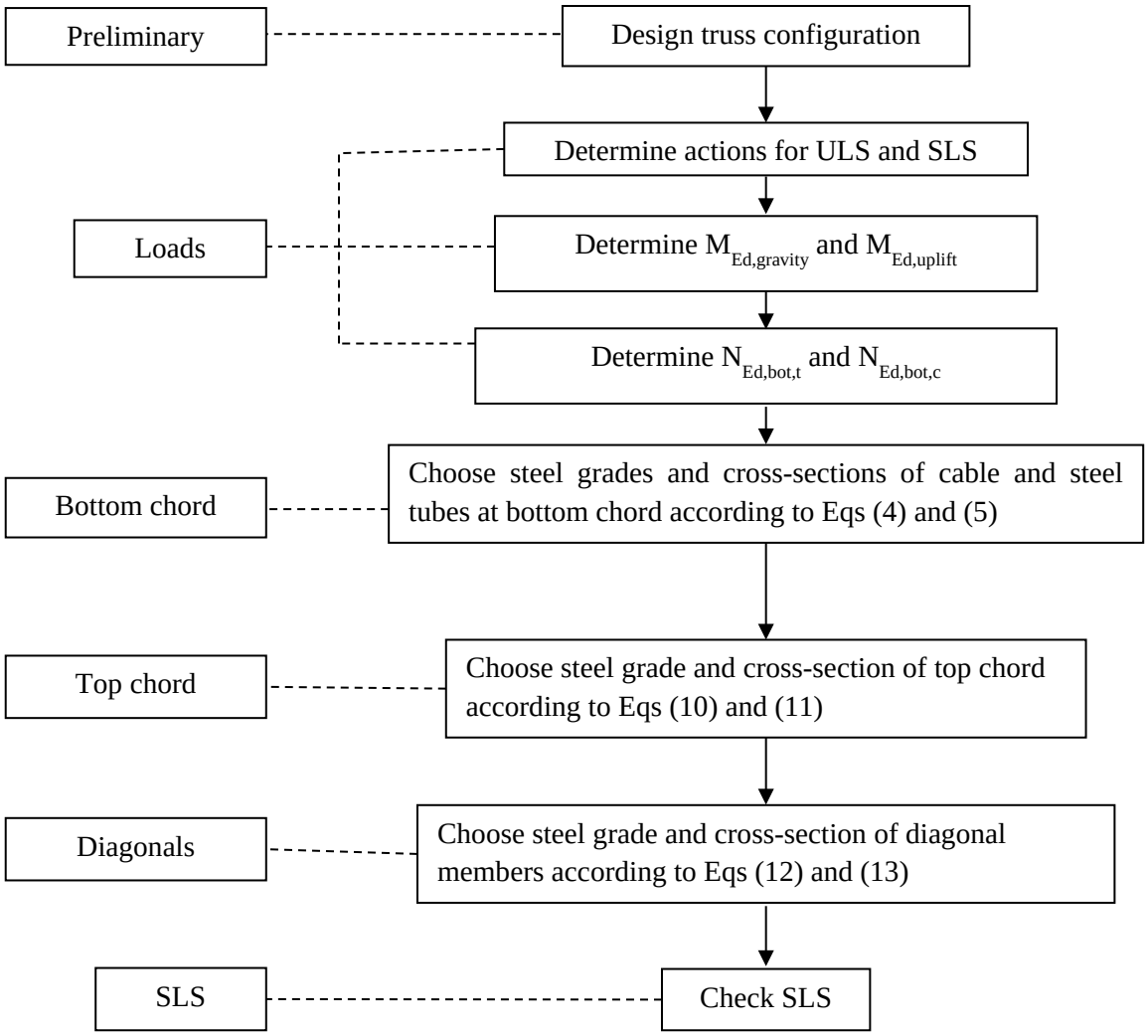

Fig. 18: Summary of simplified design checks for prestressed tubular trusses.